CHEMISTRY OF MATERIALS

pubs.acs.org/cm

Article

A Predictive Framework for Discovering Organic Metal Halide Hybrids beyond Perovskites

Kayla James,[§] Md Sazedul Islam,[§] Yufang He, Lin Wang, Jarek Viera, Elena Scivally, Spencer Schneider, Xinsong Lin, Peng Xiong, Hanwei Gao, Yan Zeng,* Biwu Ma,* and Bin Ouyang*

Cite This: https://doi.org/10.1021/acs.chemmater.5c02573

Read Online

ACCESS | Metrics & More | Article Recommendations | Supporting Information

ABSTRACT: Hybrid metal halides have transformed optoelectronics, yet predictive synthesis remains elusive beyond the perovskite family, to which the Goldschmidt tolerance factor offers guidance. Here, we present an open-source platform (https://apollo-omhh.com) that integrates a density functional theory (DFT) database of 7439 organic metal halide hybrids (OMHHs), derived from 118 experimentally reported compounds spanning diverse electronic structures. Leveraging this data set and remnant stability theory, we introduce a predictive framework to assess OMHH synthesizability. This framework successfully guided the experimental synthesis of eight previously unreported compounds and achieved an 85.2% prediction accuracy across 27 synthesis attempts. This framework is further extended to predict 268 synthesizable OMHHs among 1144 examined OMHHs. Together, these advances establish a data-driven foundation for accelerating the discovery and rational design of hybrid materials beyond perovskite structures.

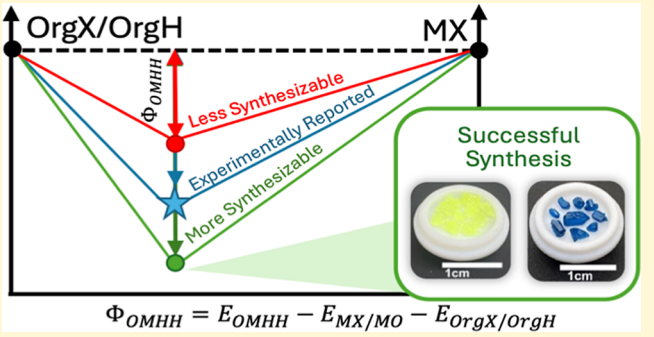

1. INTRODUCTION

The discovery of novel materials is often hindered by a limited understanding of synthesizability. While the advent of computed phase diagrams greatly drives the prediction of thermodynamic stability in inorganic compounds,[1−3] equivalent predictive frameworks for hybrid materials remain conspicuously underdeveloped. The predictive synthesis of organic metal halide hybrids (OMHHs) exemplifies this type of challenges. Organic metal halide hybrids (OMHHs), an emerging class of organic−inorganic hybrids beyond classic perovskite structures, have recently attracted great attention for their remarkable structural and property tunability, with diverse applications spanning optoelectronics, spintronics, and beyond.[4−7] Unlike the synthesis of inorganic solids,[8−13] where the competing phases are predominantly solid-state byproducts, the synthesis of OMHHs involves a delicate interplay of solid, liquid, and aqueous species. This complexity is further compounded by the lack of large-scale computational and experimental data sets that have driven progress in inorganic materials research, such as the Materials Project,[14] OQMD,[15] and NOMAD.[16]

Here, we present an open-source platform that addresses the synthesis challenges of OMHHs by integrating a comprehensive database with a predictive model for synthesizability. The APOLLO database (Advanced Photovoltaic and Optoelectronic crystaL Library of Organic Metal Halide Hybrids) is built on 118 experimentally reported zero-dimensional (0D) and one-dimensional (1D) OMHH structures and expanded via systematic ion substitutions, yielding 7439 DFT-derived entries (https://apollo-omhh.com). The online platform allows for interactive exploration of all hybrid materials within the APOLLO database, including visualization of electronic band structures and corresponding atomic structures. Users can analyze and compare band gap values across the data set, with options to visualize trends and distributions on an elemental basis. To evaluate synthetic accessibility, we developed a theoretical framework leveraging the remnant stability theory,[9,17,18] bridging solid-state DFT energetics with experimental synthesis outcomes of existing OMHHs to predict the synthesis of new OMHHs. This framework is validated by the successful synthesis of eight previously unreported OMHHs and achieves 85.2% predictive accuracy across 27 synthesis attempts. It is further applied to identify 268 synthesizable compounds among 1144 examined OMHHs. Together, these advances establish a data-driven foundation for accelerating the rational discovery of next-generation optoelectronic and spintronic technologies.

Received: September 28, 2025
Revised: November 17, 2025
Accepted: December 10, 2025

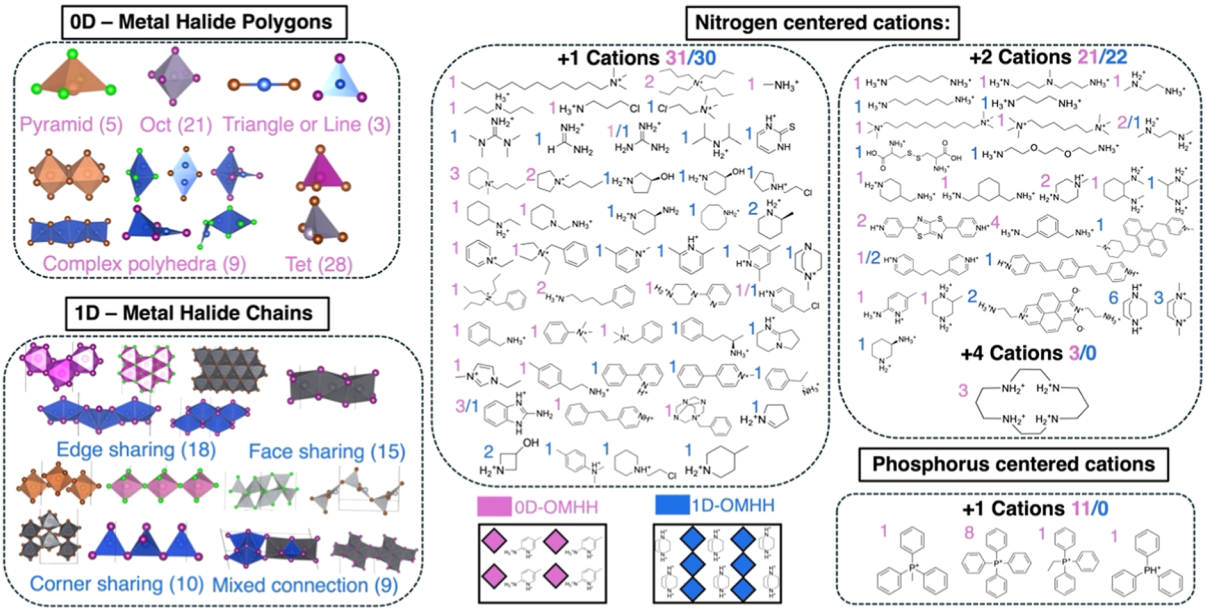

Figure 1. Structural motifs and composition statistics of OMHHs. All 0D-OMHH local motifs and their counts are shown in purple, while 1D-OMHH motifs are shown in blue. Numbers indicate the occurrences of organic and inorganic local motifs within each dimensional category, with color distinguishing between 0D and 1D structures.

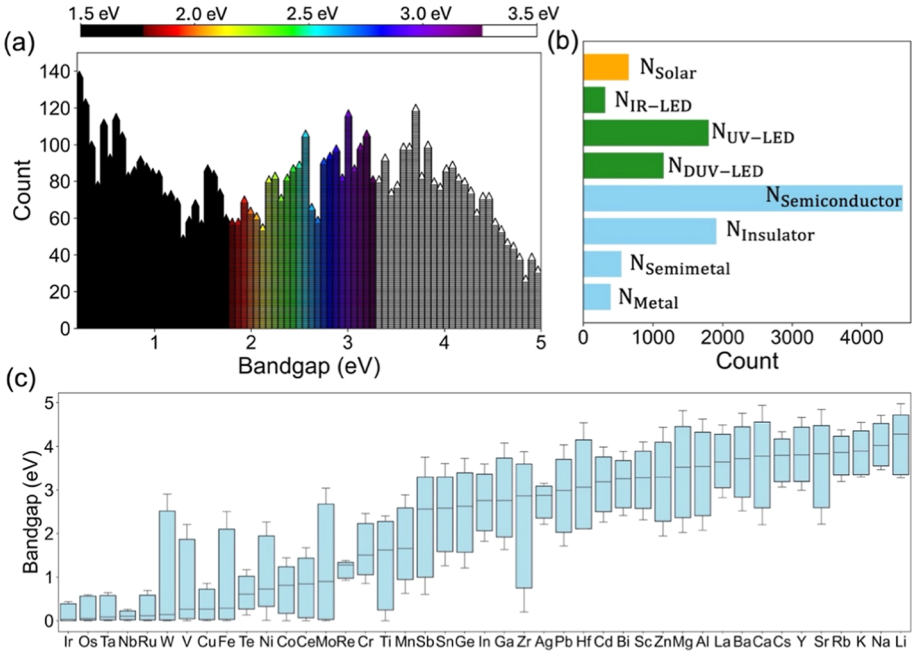

Figure 2. Statistics of electronic structures. (a) Histogram of band gaps; (b) frequencies of materials in terms of application; (c) element-dependent distribution of band gaps.

2. RESULTS AND DISCUSSION

2.1. Database with Diverse Inorganic and Organic Local Motifs. A high-throughput computational database was constructed using a curated collection of experimentally reported OMHH structures from the past decades.[19−100] We focus the scope of this work on low-dimensional hybrid materials due to their notable structural diversity[73,101,102] and corresponding enhanced photophysical properties[78,103,104] compared to high-dimensional hybrids. For example, 2D hybrids exhibit more limited structural diversity, and their structures are often predictable: monoammonium cations typically yield Ruddlesden−Popper phases, whereas diammonium cations usually lead to Dion−Jacobson structures.[105] Specifically, the data set includes 66 zero-dimensional (0D) and 52 one-dimensional (1D) OMHH structures. All 118 selected OMHH structures are fully ordered. Although some OMHH structures exhibit partial occupancies, it is highly challenging to model them with the ordered configurations required for DFT relaxation. This difficulty arises because the disorder in OMHHs primarily stems from orientational and dynamic fluctuations, rather than electrostatic interactions among different metal ions as commonly observed in inorganic compounds with compositional disorder.[106−108] Therefore, OMHH compounds with partial occupancies were excluded from this study due to their

https://doi.org/10.1021/acs.chemmater.5c02573
Chem. Mater. XXXX, XXX, XXX−XXX

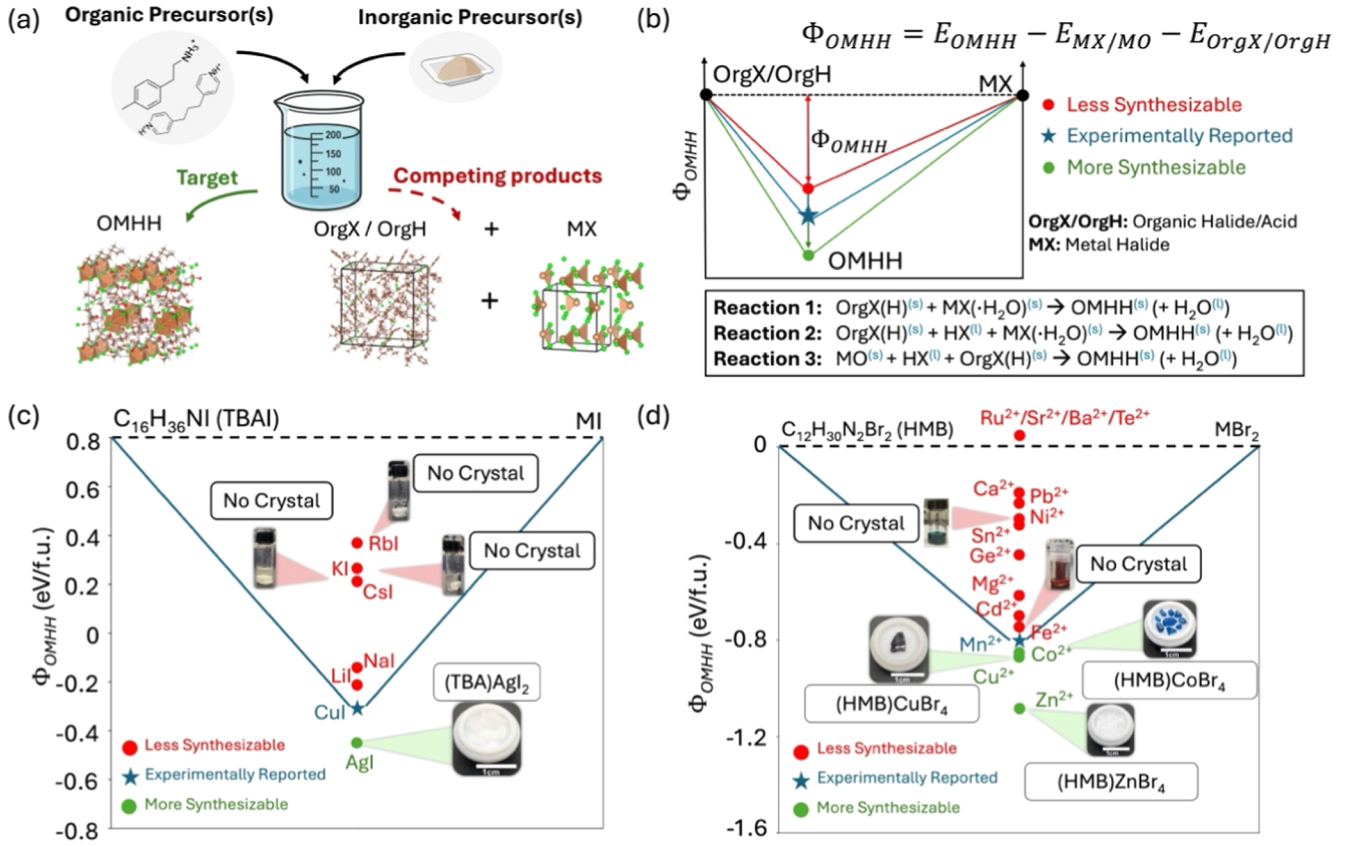

Figure 3. OMHH predictive synthesis schematic and outcomes. (a) Schematic illustration of potential solid-state competing phases during OMHH synthesis; (b) schematic definition of Φ_{OMHH}. Reaction energy maps for (c) (TBA)MI_2 and (d) (HMB)MBr_4. The experimental synthesis outcomes are indicated in the embedded images.

inherent complexity, which could distract from the main focus of our work. Systematic isovalent substitutions on metal and halogen sites were performed to generate a diverse set of hypothetical OMHHs, all of which were subjected to first-principles density functional theory (DFT) calculations (see Methodology section), resulting in a data set of 7439 structures. The database includes DFT-optimized geometries and spin-polarized band structures, accessible via the APOLLO platform (Advanced Photovoltaic and Optoelectronic crystaL Library of Organic Metal Halide Hybrids). The current form of database is mainly for ensuring the open access of the data reported in this paper, while substantial extension of user application interface development is undergoing in the near future. According to our previous benchmark,[109] the GGA/GGA + U-calculated Kohn–Sham band gap tends to agree better with optical gaps measured from experiments; we thus adopt GGA/GGA + U calculations for generating the whole database.

Figure 1 illustrates the structural diversity of both the metal halide frameworks and organic cations in OMHHs. The left panels show a range of 0D and 1D metal halide motifs, including common units such as pyramids, octahedra, tetrahedra, and triangles, as well as more complex assemblies built from these building blocks. The 1D structures feature chains formed through corner-, edge-, or face-sharing polyhedra, with additional intricate connectivity. In contrast, the organic cations, shown in the right panels, exhibit even greater diversity. Most organic cations contain nitrogen, with 40 types identified in 0D and 41 in 1D-OMHHs, while phosphorus-containing cations are also introduced in some OMHHs, with four types in 0D-OMHH structures and none in 1D-OMHHs.

2.2. Extensive Space of Electronic Structures. The creation of the computational database reveals a wide and tunable space of electronic band structures, enabling the design of diverse optoelectronic applications. Figure 2 summarizes key trends, with detailed band gap statistics by metal, halogen, and organic cation provided in supplementary Section S1. The distribution of band gaps across all 7439 OMHHs is shown in Figure 2a, color-coded by the band gap value. Furthermore, Figure 2b summarizes the number of materials suitable for different types of optoelectronic devices based on their band gap size. Among the 7439 computed OMHH structures, 393 are metallic, while 1910 are insulating with band gaps greater than 3.5 eV. The remaining 5136 are either semiconductors or semimetals. This abundance of OMHHs with small to moderate band gaps suggests a wide range of possibilities for designing optoelectronic devices, including, but not limited to, solar cells, infrared LEDs (IR-LEDs), ultraviolet LEDs (UV-LEDs), and deep-ultraviolet LEDs (DUV-LEDs), as illustrated in Figure 2b.

Element-specific band gap distributions, shown in Figure 2c, reveal several notable trends. OMHHs containing main group metals and certain early (e.g., Y, La, Sc, and Hf) and late transition metals (e.g., Zn, Cd, and Ag) predominantly exhibit insulating behavior, with band gaps typically at least 2–3 eV. This trend is largely attributed to the d^0 or d^{10} electronic configurations, which result in minimal hybridization between metal cations and halogens and large energy separations between valence and conduction bands. In d^0 systems, the conduction band arises from empty metal d orbitals; in d^{10} systems, from higher-energy s or p orbitals, while the valence band is primarily a halogen p orbital in both cases. It is worth

https://doi.org/10.1021/acs.chemmater.5c02573
Chem. Mater. XXXX, XXX, XXX−XXX

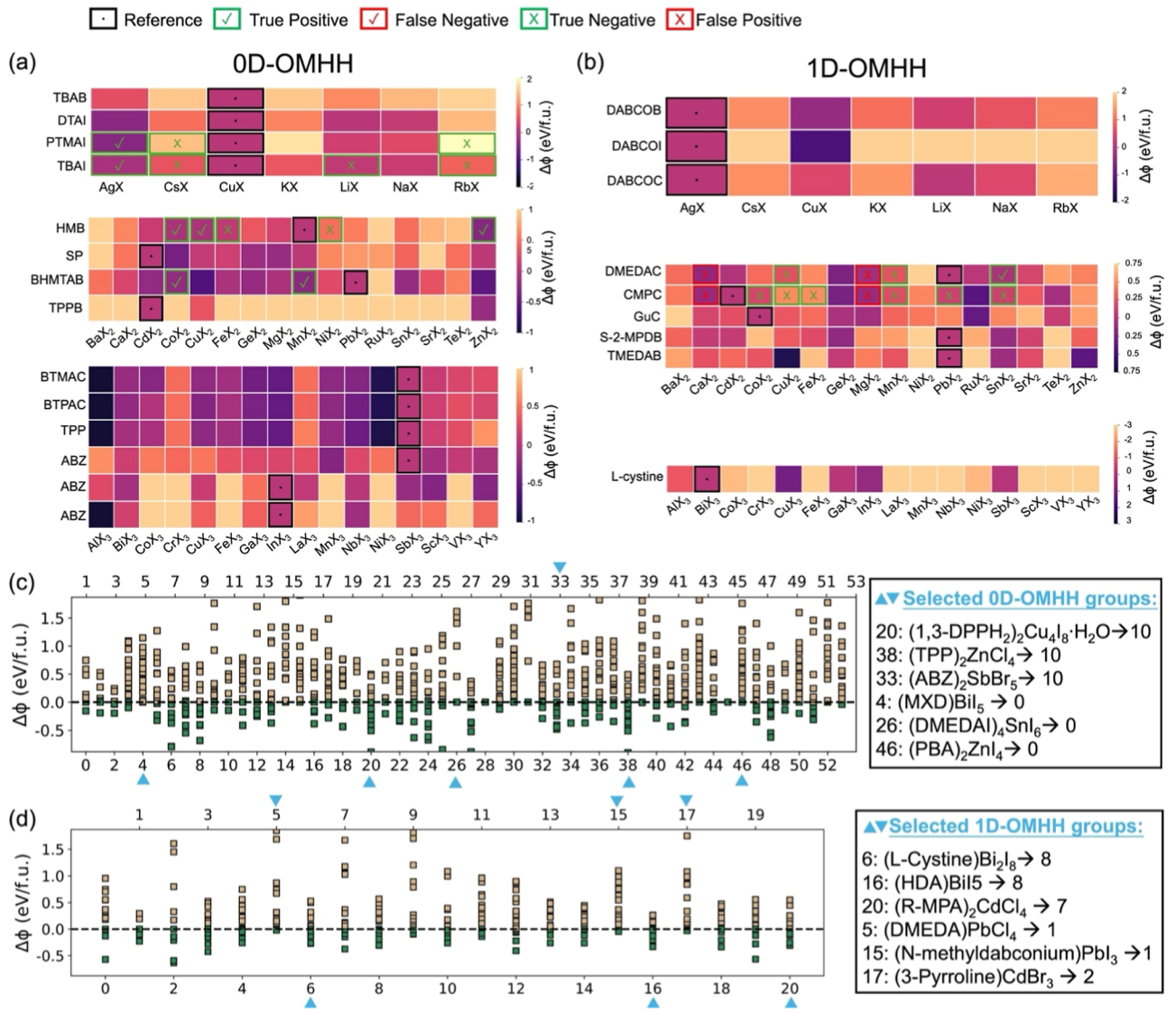

Figure 4. Relative reaction energies ($\Delta\Phi$) for 0D and 1D-OMHH synthesizability. Maps of relative reaction energies ($\Delta\Phi$) for (a) 0D-OMHH and (b) 1D-OMHH as Legendre transformations based on organic precursors and metal halides. The literature reported compounds are used as reference ($\Delta\Phi = 0$) and are outlined in a black with a central dot. Correct predictions are in green and incorrect predictions are in red. A checkmark ($\surd$) indicates the OMHH was synthesized, while an X denotes the OMHH was unable to be synthesized; (c) the $\Delta\Phi$ for 53 groups of 0D-OMHHs; (d) the $\Delta\Phi$ for 20 groups of 1D-OMHHs; both (c) and (d) are based on Legendre transformation on metal halides. Brown squares indicate data with $\Delta\Phi > 0$, while green squares indicate data with $\Delta\Phi < 0$. For clarity, only selected OMHH indices are displayed in the plots. Complete list of indices can be found in Supporting Information (section S4). The number following each arrow indicates the count of predicted OMHHs with negative $\Delta\Phi$ values for the corresponding experimental reference listed to the left of the arrow. Abbreviations: TBAB, tetrabutylammonium bromide; DTAI, dodecyltrimethylammonium iodide; PTMAI, phenyltrimethylammonium iodide; TBAI, tetrabutylammonium iodide; HMB, hexamethonium bromide, SP, 4-styrylpyridine, BHMTAB, *N*-benzylhexamethylenetetramine bromide; TPPB, tetraphenylphosphonium bromide; BTMAC, benzyltrimethylammonium chloride, BTPAC, benzyltripropylammonium chloride; TPP, triphenylphosphine; ABZ, 2-aminobenzimidazole; DABCOB, 1,4-diazabicyclo(2.2.2)octane hydrobromide; DABCOI, 1,4-diazabicyclo(2.2.2)octane hydroiodide; DABCOC, 1,4-diazabicyclo(2.2.2)-octane hydrochloride; DMEDAC, *N,N′*-dimethylethylenediammonium chloride; CMPC, 4-(chloromethyl)pyridine hydrochloride; GuC, guanidinium chloride; S-2-MPDB, S-2-methylpiperidinium bromide; TMEDAB, *N,N,N′*trimethylethylenediammonium bromide; 1,3-DPP, 1,3-di(pyridin-4-yl)propane; MXD, metaxylylenediammonium; PBA, phenylbutanammonium; HDA, 1,6-hexanediammonium; R-MPA, (R)-(−)-1-methyl-3-phenylpropylammonium; DMEDAI, *N,N′*-dimethylethylenediammonium iodide.

noting that a few outliers exist, particularly for OMHHs containing Ti^{4+} and Zr^{4+}, which show smaller-than-expected band gaps. In contrast, OMHHs with transition metals like W, V, Fe, Ni, Co, Ce, Mo, and Ti exhibit a much broader tunable range of band gaps, from metallic (0 eV) to insulating. While DFT gaps may not directly translate to optical performance, these element-dependent trends highlight the utility of electronically versatile metals in OMHH design.

2.3. Principles of Synthesizability Prediction. The database derived from curated experimental structures offers valuable opportunities to investigate OMHH synthesizability. Unlike the rapidly developed synthesis theories for pure inorganic materials,[2,3,8,110] hybrid materials lack a reliable and generalized theoretical framework for predicting their synthesizability. This is largely due to the nature of competing phases: in hybrid systems, organic components often exist as liquids. This

https://doi.org/10.1021/acs.chemmater.5c02573
Chem. Mater. XXXX, XXX, XXX−XXX

contrasts to the solid or gaseous phases typical of inorganic compounds, complicating phase stability predictions. To address this, we propose using experimentally reported OMHHs as reference points, combined with more accurate solid-state DFT calculations, to assess the likelihood of forming crystalline products. All curated OMHHs are synthesized via acid−base reactions between organic acids or salts with metal halides or oxides, producing OMHHs as salts without complex organic transformations. Halogen acids (HX) and water (H_2O) may also act as byproducts or reactants in these pathways.

Thermodynamically, the reaction energy determines the driving force for OMHH formation, defined as $E_{react} = E_{products} - E_{reactants}$. The products typically include the OMHH and, in some cases, H_2O or HX in liquid or aqueous form, while the reactants consist of organic precursor(s), inorganic precursor(s), and possibly also H_2O or HX (Figure 3a). Direct estimation of E_{react} is challenging due to the difficulty of computing energies for liquid and aqueous phases.[111−115] To circumvent this, we define a grand potential (Φ) that approximates the residual reaction energy using only solid competing phases. For the common synthetic routes shown in Figure 3b, the grand potential is defined as $\Phi_{OMHH} = E_{OMHH} - n_{MX(O)}\mu_{MX(O)} - n_{OrgX(H)}\mu_{OrgX(H)}$, where E_{OMHH} represents the total DFT energy of OMHH, and n and μ denote the number of atoms and chemical potentials of metal halides or metal oxides and organic acids/halides, respectively. As all species are solids, their energies can be reliably calculated using DFT.[2,3,110] This formulation follows the general Legendre transformation used in thermodynamics[13,14] and aligns with remnant stability theory.[17,18,116] The chemical intuition behind this approach is to capture the relative stability OMHHs against solid-state competing phase during crystallization, while the aqueous species remain the same regardless of the metal species and corresponding solid byproducts. Similar strategies have been applied in Pourbaix diagram modeling[117] and inorganic crystal formation under aqueous conditions.[116] In contrast with the criterion adopted for accessing inorganic synthesizability, we regard materials with Φ lower than experimentally reported OMHHs to be synthesizable, with full awareness that sometimes Φ slightly higher than experimentally reported compounds can also be synthesizable according to remnant stability theory.[3,9,11,12,118] However, there is much less experimental data compared to the inorganic ICSD materials for OMHH (118 curated in this work versus over 100,000 entries in ICSD), making it very difficult to come up with a convincing metastability energy scale. Therefore, we choose to focus more on materials that show Φ values lower than those of experimentally reported OMHHs as they are more accessible thermodynamically.

With the establishment of the grand potential, the OMHH synthesizability can be estimated without explicitly computing the energies of liquid or aqueous phases. This is because the relative grand potential, $\Delta\Phi$, inherently cancels out contributions from common solvents such as HX or H_2O when comparing synthesis reactions of the same type. A lower Φ_{OMHH} relative to that of an experimentally reported compound (Φ^{Exp}_{OMHH}) suggests a more exergonic reaction and thus a higher likelihood of successful synthesis. To validate this framework, we conducted systematic synthesis attempts in two selected OMHH chemical spaces (Figure 3c and d). In Figure 3c, TBAI ($C_{16}H_{36}NI$, tetrabutylammonium iodide) was reacted with various +1 metal halides to attempt the formation of OMHHs. DFT calculations indicated that only (TBA)AgI_2 has a lower Φ_{OMHH} than the known (TBA)CuI_2.[58] Experimental synthesis attempts with Ag^+, Cs^+, K^+, and Rb^+ confirmed that only (TBA)AgI_2 formed successfully, which is fully consistent with the predictions. Figure 3d explores reactions between HMB ($C_6H_{15}NBr$, hexamethonium bromide) and +2 metal halides. Among 16 evaluated M^{2+} cations, Co^{2+}, Cu^{2+}, and Zn^{2+} were predicted to yield OMHHs with lower Φ_{OMHH} values than the known Mn^{2+} compound. All three were successfully synthesized, while the predicted failures, Fe^{2+} and Ni^{2+} OMHHs, could not be obtained. These 9 out of 9 accurate predictions across these two distinct OMHH groups highlight the robustness and reliability of our synthesizability prediction framework.

2.4. Experimental Validation of the Relative Grand Potential Framework. When comparing OMHHs synthesized via the same reaction schemes but differing in metal identify, variations in reaction energy can be effectively captured by the relative grand potential between Φ_{OMHH} and its experimental counterpart Φ^{Exp}_{OMHH}, denoted as $\Delta\Phi$. As shown in Figure 3, Φ_{OMHH} is expressed as the Legendre transformation of the total energy of the OMHH with respect to its solid organic precursors and metal halides. Beyond the examples in Figure 3c and d, we expanded our analysis to 23 of the 118 OMHH frameworks, generating predictions for 305 OMHHs (188 0D-OMHHs and 117 1D-OMHHs). A list of examined compounds is provided in Supporting Information Section S5. Among 0D-OMHHs, 3 of 28 M^+, 16 of 64 M^{2+}, and 39 of 96 M^{3+} variants exhibit negative $\Delta\Phi$ values, indicating greater thermodynamic favorability than the experimental reference. Similarly, for 1D-OMHHs, 2 of 21 M^+, 18 of 80 M^{2+}, and 3 of 16 M^{3+} systems show negative $\Delta\Phi$. These trends are summarized in Figure 4a and b as heatmaps grouped by metal valence and dimensionality. Guided by these predictions, 27 synthesis attempts were conducted, yielding 23 successful outcomes and 4 failures, demonstrating 85.2% predictive accuracy. Convex hull analyses for all compounds beyond those in Figure 3 are provided in supplementary Section S2, with exact reaction energies provided in supplementary section S3.

For OMHHs synthesized from liquid organic precursors and solid metal halides or oxides, an alternative definition of Φ_{OMHH} can be chosen as $\Phi_{OMHH} = E_{OMHH} - n_{MX(O)}\mu_{MX(O)}$. This form remains valid for comparing reaction energies among OMHHs of identical stoichiometry but different metal species, as organic contributions cancel out, allowing consistent evaluation across varying metal precursors and competing products, e.g., metal halides or oxides. This alternative definition broadens the applicability of Φ_{OMHH} and enables the assessment of 1144 OMHHs in our databases. The resulting $\Delta\Phi$ distributions are shown in Figure 4c and d. Due to the large number of compounds, only selected OMHHs are labeled explicitly, while the complete list is available in supplementary section S4. Based on this analysis, 176 of 801 0D-OMHHs and 92 of 343 1D-OMHHs are predicted to be more synthesizable (i.e., exhibit negative $\Delta\Phi$). The top three most and least synthesizable OMHHs in each dimensional category are highlighted in the figure legends as representative examples.

While our framework demonstrates strong predictive performance, it is not without limitations. Among the four incorrect predictions across 27 experimental attempts, all four involve reactions with $CaCl_2$ and $MgCl_2$, where the model does not capture the experimental outcome. In these cases, the key challenge lies in identifying an antisolvent that effectively

https://doi.org/10.1021/acs.chemmater.5c02573
Chem. Mater. XXXX, XXX, XXX−XXX

suppresses the solubility of both ammonium ions and Ca^{2+}/Mg^{2+}, a factor not currently accounted for by the theoretical framework. Due to the limitation of data and substantial effort to further explore the solubility of ions and the hydration process during the synthesis, further improvements could incorporate experimental measurements of solubility limits across various solvents, following approaches used for inorganic systems,[117,119] to further enhance predictive accuracy. Moreover, the current framework primarily focuses on assessing the likelihood of precipitating a solid OMHH phase from aqueous solution, but it has a limited capability to predict the competition among potential polymorphs due to the lack of comprehensive experimental references and crystal structure data. A tighter integration between structural search algorithms and experimental design could be an exciting next step toward exploring this largely underdeveloped material space. Finally, kinetic factors are always important regardless of the materials synthesis type, which should also apply in OMHHs. Leveraging the existing thermodynamic data set established in this work and further extending it to consider kinetic factors will be a potential exciting next step for the OMHH community.

3. CONCLUSION

We present a comprehensive data-driven framework for exploring organic metal halide hybrids (OMHHs) beyond traditional perovskite structures. Built on a high-throughput DFT-screened database of experimentally derived structures, the framework leverages structural and electronic property data to predict OMHH synthesizability. Validated through 27 experimental attempts with 85.2% accuracy, this approach provides a robust foundation for high-throughput and rational synthetic exploration across a broad class of hybrid materials, which also yield 268 synthesizable OMHHs among 1144 examined OMHHs.

4. METHODOLOGY

4.1. Electronic Structure Calculations. All electronic structure calculations were performed using the Vienna Ab-initio Simulation Package (VASP)[120−122] with PBE functionals[123] and PAW pseudopotentials.[124,125] A reciprocal space discretization of 25 k-points per $Å^{-1}$ was used to sample the Brillouin zone.[126] The kinetic energy cutoff was 520 eV. The Methfessel−Paxton scheme was used to smooth the partial occupancies for each orbital,[127] with a smearing width of 0.2 eV. The convergence criterion for the self-consistent field (SCF) step was 10^{-5} eV/atom. Geometric optimizations were executed until the force on each atom was less than 0.05 eV. Hubbard U corrections[128,129] were applied to Fe, Mn, and V with values of 5.3, 3.9, and 3.25 eV, respectively, following values established in previous works.[11,130]

5. MATERIALS

Copper(II) chloride ($CuCl_2$, 97.0%), manganese(II) chloride ($MnCl_2$, 99.0%), iron(II) chloride ($FeCl_2$, 99.9%), cobalt(II) chloride ($CoCl_2$, 97.0%), calcium chloride ($CaCl_2$, 97.0%), magnesium chloride ($MgCl_2$, 98.0%), tin(II) chloride ($SnCl_2$, 98.0%), lead(II) chloride ($PbCl_2$, 98.0%), copper(II) bromide ($CuBr_2$, 99.0%), cobalt(II) bromide ($CoBr_2$, 99.0%), manganese(II) bromide ($MnBr_2$, 98.0%), iron(II) bromide ($FeBr_2$, 98.0%), zinc(II) bromide ($ZnBr_2$, 98.0%), nickel(II) bromide ($NiBr_2$, 98.0%), silver iodide (AgI, 99.9%), lithium iodide (LiI, 98.0%), rubidium iodide (RbI, 99.9%), cesium iodide (CsI, 99.9%), tetrabutylammonium iodide (TBAI, $C_{16}H_{36}NI$, 98.0%), hexamethonium bromide (HMB, $C_{12}H_{30}N_2Br_2$, 98.0%), 4-(chloromethyl)-pyridine hydrochloride (CMP, $C_6H_6ClN.HCl$, 97.0%), benzyl bromide ($C_6H_5CH_2Br$, 98.0%), hexamethylenetetramine ($C_6H_{12}N_4$, 99.0%), *N*,*N*′-dimethylethylenediamine (DMEDA, $C_4H_{12}N_2$, 98.0%), dimethylformamide (DMF, 99.8%), dichloromethane (DCM, 99.9%), hydrochloric acid (HCl, 37.0%), hydrobromic acid (HBr, 48.0%), and ethanol (200 proof) were purchased from MilliporeSigma. Phenyltrimethylammonium iodide (PTMAI, $C_9H_{14}NI$, 98.0%) was purchased from Fisher Scientific. All of the reagents and solvents were used without further purification.

5.1. Synthesis of $(TBA)_3Ag_3I_6$. TBAI (1 mmol) and AgI (1 mmol) were dissolved in 1 mL of DMF to form a clear precursor solution. Single crystals of the hybrid were obtained after a few days by slowly evaporating the solvent at room temperature in a fume hood. The crystals were washed with diethyl ether and dried under reduced pressure. Attempts to synthesize hybrids of TBAI with LiI, RbI, and CsI using the same method were unsuccessful.

5.2. Synthesis of (HMB)$CoBr_4$, (HMB)$CuBr_4$, and (HMB)$ZnBr_4$. HMB (1 mmol) and $CoBr_2$ (1 mmol) were dissolved into a desired amount of HBr (48%) and deionized water under vigorous stirring. Single crystals of the hybrid were obtained after a few days by slow evaporation of the above solution at room temperature in a fume hood. Single crystals of the (HMB)$CuBr_4$ and (HMB)$ZnBr_4$ hybrids were also synthesized using the same procedure but replacing $CoBr_2$ with corresponding metal halides. All of the crystals were washed with diethyl ether and dried under reduced pressure. Attempts to synthesize hybrids of HMB with $FeBr_2$ and $NiBr_2$ using the same method were unsuccessful.

5.3. Synthesis of $(BHMTA)_2MnBr_4$ and $(BHMTA)_2CoBr_4$. First, BHMTAB ($C_{13}H_{19}N_4Br$) salt was prepared by mixing benzyl bromide (7.0 mmol) with hexamethylenetetramine (7.0 mmol) in 150 mL of ethanol at 0 °C. The white organic salts were obtained after filtration under vacuum. The salts were washed with ethanol and dried under reduced pressure. To synthesize the hybrid, *N*-benzyl hexamethylenetetramine bromide (0.4 mmol) and $MnBr_2$ (0.2 mmol) were dissolved in a mixed solvent of methanol (2.0 mL) and acetonitrile (2.0 mL) under vigorous stirring to form a clear solution. Single crystals of the hybrid were obtained in 2 days by slowly evaporating the solvent at room temperature in a fume hood. Single crystals of the $(BHMTA)_2CoBr_4$ hybrid were also synthesized using the same procedure but replacing $MnBr_2$ with $CoBr_2$. All of the crystals were washed with diethyl ether and dried under reduced pressure.

5.4. Synthesis of $(PTMA)AgI_2$. PTMAI (1 mmol) and AgI (1 mmol) were dissolved in 1 mL of dimethylformamide (DMF) to form a clear precursor solution. Single crystals of the hybrid were obtained after a few days by slowly evaporating the DMF solvent at room temperature in a fume hood. The crystals were washed with diethyl ether and dried under reduced pressure. Attempts to synthesize hybrids of PTMAI with RbI and CsI using the same method were unsuccessful.

5.5. Synthesis of $(DMEDA)SnCl_4$. First, the DMEDAC ($C_4H_{14}N_2Cl_2$) salt was prepared by dissolving *N*,*N*′-dimethylethylenediamine (7.0 mmol) in 80.0 mL of ethanol, followed by the dropwise addition of 1.26 mL of HCl (37%) at 0 °C, and stirring for 1 h. The white organic salts were obtained after filtration under vacuum. The salts were washed with a suitable amount of diethyl ether and dried under reduced pressure. To synthesize the hybrid, $C_4H_{14}N_2Cl_2$ (1 mmol) and $SnCl_2$ (1 mmol) were dissolved in 1 mL of DMF in a small vial to form a clear precursor solution. Then the small vial was placed in a large vial with 10 mL of DCM inside it. Colorless block crystals were obtained by leaving the vial to stand for around 2 days. The crystals were washed with DCM and dried under reduced pressure. Attempts to synthesize hybrids of DMEDAC with $CuCl_2$, $MnCl_2$, $CaCl_2$, and $MgCl_2$ using the same method were unsuccessful.

5.6. Synthesis of CMP-Metal Halide Hybrids. CMP-metal halide hybrids were attempted to synthesize by the solvent evaporation method described by Xu et al.[37] 1 mmol of CMPC was separately mixed with 1 mmol of 8 different metal chlorides ($CuCl_2$, $MnCl_2$, $CaCl_2$, $MgCl_2$, $SnCl_2$, $FeCl_2$, $CoCl_2$, and $PbCl_2$) in 1 mL of deionized water. The solutions were left to evaporate at 30 °C for 7 days, but no crystallization of the hybrids was observed.

5.7. Single-Crystal X-ray Diffraction (SCXRD). The single-crystal structures of the synthesized hybrids were solved using a Rigaku

https://doi.org/10.1021/acs.chemmater.5c02573
Chem. Mater. XXXX, XXX, XXX−XXX

XtaLAB Synergy-S diffractometer equipped with a Cu microfocus sealed tube X-ray source (wavelength = 1.54 Å) and a HyPix-6000HE Hybrid Photon Counting (HPC) detector. A crystal of suitable size was mounted in a cryoloop with Paratone-N oil. The data were collected by maintaining the temperature at 150 K using an Oxford-Diffraction Cryojet. Olex2 software2[131] was used to solve the crystal structure with the SHELXT3[132] structure solution program using Intrinsic Phasing, and SHELXL3[132] refinement package was used to refine the data using Least Squares minimization. The crystal data and structure refinement details of the synthesized hybrids are summarized in Tables S4−S8. The images of crystal structures presented in this manuscript were drawn using VESTA as the crystal structure visualization software. Single-crystal XRD refinements results are demonstrated in Section S5.

■ ASSOCIATED CONTENT

Data Availability Statement

All data supporting the findings are available in the main text or the Supporting Information. The APOLLO database is available at https://apollo-omhh.com.

Supporting Information

The Supporting Information is available free of charge at https://pubs.acs.org/doi/10.1021/acs.chemmater.5c02573.

Additional convex hull diagrams, single-crystal X-ray diffraction details, and elemental band gap heatmaps (PDF)

Table S1: Tabulated Reaction Energies of Proposed OMHHs (XLSX)

Accession Codes

Deposition Numbers 2439818, 2439825, 2444866, 2446472, 2453732, 2471415, 2473731, and 2474962 contain the supplementary crystallographic data for this paper. These data can be obtained free of charge via the joint Cambridge Crystallographic Data Centre (CCDC) and Fachinformations-zentrum Karlsruhe Access Structures service.

■ AUTHOR INFORMATION

Corresponding Authors

Yan Zeng − *Department of Chemistry and Biochemistry, Florida State University, Tallahassee, Florida 32304, United States;* orcid.org/0000-0002-5831-1210; Email: zeng@chem.fsu.edu

Biwu Ma − *Department of Chemistry and Biochemistry, Florida State University, Tallahassee, Florida 32304, United States;* orcid.org/0000-0003-1573-8019; Email: bma@fsu.edu

Bin Ouyang − *Department of Chemistry and Biochemistry, Florida State University, Tallahassee, Florida 32304, United States;* orcid.org/0000-0002-8181-6815; Email: bouyang@fsu.edu

Authors

Kayla James − *Department of Chemistry and Biochemistry, Florida State University, Tallahassee, Florida 32304, United States;* orcid.org/0009-0005-0187-4732

Md Sazedul Islam − *Department of Chemistry and Biochemistry, Florida State University, Tallahassee, Florida 32304, United States*

Yufang He − *Department of Chemistry and Biochemistry, Florida State University, Tallahassee, Florida 32304, United States*

Lin Wang − *Department of Chemistry and Biochemistry, Florida State University, Tallahassee, Florida 32304, United States*

Jarek Viera − *Department of Chemistry and Biochemistry, Florida State University, Tallahassee, Florida 32304, United States*

Elena Scivally − *Department of Chemistry and Biochemistry, Florida State University, Tallahassee, Florida 32304, United States;* orcid.org/0009-0008-8138-550X

Spencer Schneider − *Department of Chemistry and Biochemistry, Florida State University, Tallahassee, Florida 32304, United States*

Xinsong Lin − *Department of Chemistry and Biochemistry, Florida State University, Tallahassee, Florida 32304, United States*

Peng Xiong − *Department of Physics, Florida State University, Tallahassee, Florida 32304, United States*

Hanwei Gao − *Department of Physics, Florida State University, Tallahassee, Florida 32304, United States;* orcid.org/0000-0001-8085-8178

Complete contact information is available at: https://pubs.acs.org/10.1021/acs.chemmater.5c02573

Author Contributions

[§]K.J. and M.S.I. contributed equally to this work. B.O., B.M., and Y.Z. designed this project, B.O., K.J., and Y.H., performed computational analysis, M.S.I. did all experiments and analyzed all experimental data; all authors contributed to the discussion of the paper as well as writing the paper.

Notes

The authors declare no competing financial interest.

■ ACKNOWLEDGMENTS

This research was supported in part by Florida State University (FSU) Seed Grants led by H.G. and B.O., as well as by NSF Grant CHE-2500487 (PIs: B.M. and B.O.). M.S.I., J.V., and B.M. acknowledge additional support from the National Science Foundation under Award No. DMR-2204466. Contributions from the research groups of Y.Z. and B.O. were also supported by FSU startup funds. P.X. acknowledges support from NSF Grant DMR-2325147. Additional support was provided by FSU Seed Grants led by P.X. and B.M. The Computational resources are provided by the Advanced Cyberinfrastructure Coordination Ecosystem: Services & Support (ACCESS), the National Energy Research Scientific Computing Center (NERSC), a DOE Office of Science User Facility supported by the Office of Science and the U.S. Department of Energy under contract no. DE-AC02-05CH11231 and Research Computing Center (RCC) at Florida State University. The computation and data processing are also supported by the supercomputing resources from the Department of Energy's Office of Energy Efficiency and Renewable Energy at the National Renewable Energy Laboratory. This work made use of the Rigaku Synergy-S single-crystal X-ray diffractometer that was acquired through the NSF MRI program (CHE-1828362).

■ REFERENCES

(1) Gibbs, J. W. On the equilibrium of heterogeneous substances. *Am. J. Sci.* **1878**, *s3−16* (96), 441−458.

(2) Ong, S. P.; Wang, L.; Kang, B.; Ceder, G. Li−Fe−P−O2 Phase Diagram from First Principles Calculations. *Chem. Mater.* **2008**, *20* (5), 1798−1807.

(3) Sun, W.; Dacek, S. T.; Ong, S. P.; Hautier, G.; Jain, A.; Richards, W. D.; Gamst, A. C.; Persson, K. A.; Ceder, G. The thermodynamic scale of inorganic crystalline metastability. *Sci. Adv.* **2016**, *2* (11), No. e1600225.

(4) Lin, H.; Zhou, C.; Tian, Y.; Siegrist, T.; Ma, B. Low-Dimensional Organometal Halide Perovskites. *ACS Energy Lett.* **2018**, *3* (1), 54−62.
(5) Zhou, C.; Lin, H.; Lee, S.; Chaaban, M.; Ma, B. Organic−inorganic metal halide hybrids beyond perovskites. *Mater. Res. Lett.* **2018**, *6* (10), 552−569.
(6) Zhou, C.; Lin, H.; He, Q.; Xu, L.; Worku, M.; Chaaban, M.; Lee, S.; Shi, X.; Du, M.-H.; Ma, B. Low dimensional metal halide perovskites and hybrids. *Mater. Sci. Eng., R* **2019**, *137*, 38−65.
(7) Zhou, C.; Xu, L.-J.; Lee, S.; Lin, H.; Ma, B. Recent Advances in Luminescent Zero-Dimensional Organic Metal Halide Hybrids. *Adv. Opt. Mater.* **2021**, *9* (18), 2001766.
(8) Bianchini, M.; Wang, J.; Clément, R. J.; Ouyang, B.; Xiao, P.; Kitchaev, D.; Shi, T.; Zhang, Y.; Wang, Y.; Kim, H.; et al. The interplay between thermodynamics and kinetics in the solid-state synthesis of layered oxides. *Nat. Mater.* **2020**, *19* (10), 1088−1095.
(9) Wang, L.; He, Z.; Ouyang, B. Data driven design of compositionally complex energy materials. *Comput. Mater. Sci.* **2023**, *230*, 112513.
(10) Patil, S.; Darbar, D.; Self, E. C.; Malkowski, T.; Wu, V. C.; Giovine, R.; Szymanski, N. J.; McAuliffe, R. D.; Jiang, B.; Keum, J. K.; et al. Alternate Synthesis Method for High-Performance Manganese Rich Cation Disordered Rocksalt Cathodes. *Adv. Energy Mater.* **2023**, *13* (4), 2203207.
(11) Wang, L.; Sunariwal, N.; He, Y.; Kim, D.-h.; Yeon, D.-h.; Zeng, Y.; Cabana, J.; Ouyang, B. Elemental Stability Rules for High Entropy Disordered Rocksalt Type Li-Ion Battery Positive Electrodes. *Adv. Energy Mater.* **2025**, *15* (22), 2404982.
(12) Wang, L.; Wang, J.; Ouyang, B. Computational Investigation of MAX as Intercalation Host for Rechargeable Aluminum-Ion Battery. *Adv. Energy Mater.* **2023**, *13* (46), 2302584.
(13) Wang, L.; Ouyang, B. Phase Selection Rules of Multi-Principal Element Alloys. *Adv. Mater.* **2024**, *36* (16), 2307860.
(14) Jain, A.; Ong, S. P.; Hautier, G.; Chen, W.; Richards, W. D.; Dacek, S.; Cholia, S.; Gunter, D.; Skinner, D.; Ceder, G.; et al. Commentary: The Materials Project: A materials genome approach to accelerating materials innovation. *APL Mater.* **2013**, *1* (1), 011002.
(15) Saal, J. E.; Kirklin, S.; Aykol, M.; Meredig, B.; Wolverton, C. Materials Design and Discovery with High-Throughput Density Functional Theory: The Open Quantum Materials Database (OQMD). *JOM* **2013**, *65* (11), 1501−1509.
(16) Draxl, C.; Scheffler, M. The NOMAD laboratory: from data sharing to artificial intelligence. *J. Phys.: Mater.* **2019**, *2* (3), 036001.
(17) Alberty, R. A. Legendre Transforms in Chemical Thermodynamics. *Chem. Rev.* **1994**, *94* (6), 1457−1482.
(18) Zia, R. K. P.; Redish, E. F.; McKay, S. R. Making sense of the Legendre transform. *Am. J. Phys.* **2009**, *77* (7), 614−622.
(19) Zhuang, J.-C.; Tan, Y.-H.; Fan, X.-W.; Tang, Y.-Z.; Song, N.; Zhang, Y.-H.; Zhang, H.; Chen, S.-P. A 1D chiral infinite chain organic metal halide hybrid with excellent SHG switching and moderate spontaneous polarization. *New J. Chem.* **2022**, *46* (15), 7103−7107.
(20) Zhu, S.; Pan, J.; Chen, X.; Chen, H.; Pan, S. Solution growth and optical properties of lead-free highly efficient green-emitting [Emim]-4[Cu4I8] single crystals with 0D structure. *J. Lumin.* **2023**, *253*, 119467.
(21) Zhou, G.; Jiang, X.; Molokeev, M.; Lin, Z.; Zhao, J.; Wang, J.; Xia, Z. Optically Modulated Ultra-Broad-Band Warm White Emission in Mn2+-Doped (C6H18N2O2)PbBr4 Hybrid Metal Halide Phosphor. *Chem. Mater.* **2019**, *31* (15), 5788−5795.
(22) Zhou, C.; Worku, M.; Neu, J.; Lin, H.; Tian, Y.; Lee, S.; Zhou, Y.; Han, D.; Chen, S.; Hao, A.; et al. Facile Preparation of Light Emitting Organic Metal Halide Crystals with Near-Unity Quantum Efficiency. *Chem. Mater.* **2018**, *30* (7), 2374−2378.
(23) Zhou, C.; Lin, H.; Tian, Y.; Yuan, Z.; Clark, R.; Chen, B.; van de Burgt, L. J.; Wang, J. C.; Zhou, Y.; Hanson, K.; et al. Luminescent zero-dimensional organic metal halide hybrids with near-unity quantum efficiency. *Chem. Sci.* **2018**, *9* (3), 586−593.
(24) Zhou, C.; Lin, H.; Shi, H.; Tian, Y.; Pak, C.; Shatruk, M.; Zhou, Y.; Djurovich, P.; Du, M.-H.; Ma, B. A Zero-Dimensional Organic Seesaw-Shaped Tin Bromide with Highly Efficient Strongly Stokes-Shifted Deep-Red Emission. *Angew. Chem.* **2017**, *130* (4), 1033−1036.
(25) Zheng, Y.; Xu, J.; Bu, X.-H. 1D Chiral Lead Halide Perovskites with Superior Second-Order Optical Nonlinearity. *Adv. Opt. Mater.* **2022**, *10* (1), 2101545.
(26) Zhao, J.-Q.; Shi, H.-S.; Zeng, L.-R.; Ge, H.; Hou, Y.-H.; Wu, X.-M.; Yue, C.-Y.; Lei, X.-W. Highly emissive zero-dimensional antimony halide for anti-counterfeiting and confidential information encryption-decryption. *Chem. Eng. J.* **2022**, *431*, 134336.
(27) Zhang, Z.; Liao, J.-F.; Xing, G. Regulating the coordination geometry of polyhedra in zero-dimensional metal halides for tunable emission. *Nanoscale* **2023**, *15* (11), 5241−5248.
(28) Zhang, W.-F.; Pan, W.-J.; Xu, T.; Song, R.-Y.; Zhao, Y.-Y.; Yue, C.-Y.; Lei, X.-W. One-Dimensional Face-Shared Perovskites with Broad-Band Bluish White-Light Emissions. *Inorg. Chem.* **2020**, *59* (19), 14085−14092.
(29) Zhang, W.; Tao, K.; Ji, C.; Sun, Z.; Han, S.; Zhang, J.; Wu, Z.; Luo, J. (C6H13N)2BiI5: A One-Dimensional Lead-Free Perovskite-Derivative Photoconductive Light Absorber. *Inorg. Chem.* **2018**, *57* (8), 4239−4243.
(30) Zhang, S.; Zhao, Y.; Zhou, J.; Ming, H.; Wang, C.-H.; Jing, X.; Ye, S.; Zhang, Q. Structural design enables highly-efficient green emission with preferable blue light excitation from zero-dimensional manganese (II) hybrids. *Chem. Eng. J.* **2021**, *421*, 129886.
(31) Yue, C.-Y.; Sun, C.; Li, D.-Y.; Dong, Y.-H.; Wang, C.-L.; Zhao, H.-F.; Jiang, H.; Jing, Z.-H.; Lei, X.-W. Organic−Inorganic Hybrid Heterometallic Halides with Low-Dimensional Structures and Red Photoluminescence Emissions. *Inorg. Chem.* **2019**, *58* (15), 10304−10312.
(32) Yue, C.-Y.; Lin, N.; Gao, L.; Jin, Y.-X.; Liu, Z.-Y.; Cao, Y.-Y.; Han, S.-S.; Lian, X.-K.; Hu, B.; Lei, X.-W. Organic cation directed one-dimensional cuprous halide compounds: syntheses, crystal structures and photoluminescence properties. *Dalton Trans.* **2019**, *48* (27), 10151−10159.
(33) Yao, L.; Zeng, Z.; Cai, C.; Xu, P.; Gu, H.; Gao, L.; Han, J.; Zhang, X.; Wang, X.; Wang, X.; et al. Strong Second- and Third-Harmonic Generation in 1D Chiral Hybrid Bismuth Halides. *J. Am. Chem. Soc.* **2021**, *143* (39), 16095−16104.
(34) Xue, C.; Yao, Z.-Y.; Zhang, J.; Liu, W.-L.; Liu, J.-L.; Ren, X.-M. Extra thermo- and water-stable one-dimensional organic−inorganic hybrid perovskite [N-methyldabconium]PbI3 showing switchable dielectric behaviour, conductivity and bright yellow-green emission. *Chem. Commun.* **2018**, *54* (34), 4321−4324.
(35) Xu, T.; Li, Y.; Nikl, M.; Kucerkova, R.; Zhou, Z.; Chen, J.; Sun, Y.-Y.; Niu, G.; Tang, J.; Wang, Q.; et al. Lead-Free Zero-Dimensional Organic-Copper(I) Halides as Stable and Sensitive X-ray Scintillators. *ACS Appl. Mater. Interfaces* **2022**, *14* (12), 14157−14164.
(36) Xu, L.-J.; Plaviak, A.; Lin, X.; Worku, M.; He, Q.; Chaaban, M.; Kim, B. J.; Ma, B. Metal Halide Regulated Photophysical Tuning of Zero-Dimensional Organic Metal Halide Hybrids: From Efficient Phosphorescence to Ultralong Afterglow. *Angew. Chem.* **2020**, *132* (51), 23267−23271.
(37) Xu, H.; Zhang, Z.; Dong, X.; Huang, L.; Zeng, H.; Lin, Z.; Zou, G. Corrugated 1D Hybrid Metal Halide [C6H7ClN]CdCl3 Exhibiting Broadband White-Light Emission. *Inorg. Chem.* **2022**, *61* (11), 4752−4759.
(38) Wu, S.; Zhou, B.; Yan, D. Low-Dimensional Organic Metal Halide Hybrids with Excitation-Dependent Optical Waveguides from Visible to Near-Infrared Emission. *ACS Appl. Mater. Interfaces* **2021**, *13* (22), 26451−26460.
(39) Wu, J.; Guo, Y.; Qi, J.-L.; Yao, W.-D.; Yu, S.-X.; Liu, W.; Guo, S.-P. Multi-Stimuli Responsive Luminescence and Domino Phase Transition of Hybrid Copper Halides with Nonlinear Optical Switching Behavior. *Angew. Chem., Int. Ed.* **2023**, *62* (18), No. e202301937.
(40) Wu, G.; Zhou, C.; Ming, W.; Han, D.; Chen, S.; Yang, D.; Besara, T.; Neu, J.; Siegrist, T.; Du, M.-H.; et al. A One-Dimensional Organic Lead Chloride Hybrid with Excitation-Dependent Broadband Emissions. *ACS Energy Lett.* **2018**, *3* (6), 1443−1449.
(41) Wu, F.; Wei, Q.; Li, X.; Liu, Y.; Huang, W.; Chen, Q.; Li, B.; Luo, J.; Liu, X. Cooperative Enhancement of Second Harmonic Generation

https://doi.org/10.1021/acs.chemmater.5c02573
Chem. Mater. XXXX, XXX, XXX−XXX

in an Organic−Inorganic Hybrid Antimony Halide. *Cryst. Growth Des.* **2022**, *22* (6), 3875−3881.
(42) Wei, X.; He, J.; Zhu, Y.; Qin, Z.; Zheng, G.; Zhang, R.; Mo, S.; Wang, J.; Yao, D.; Lin, B.; et al. Synthesis, structure, and photoelectric properties of a novel zero-dimensional organic-inorganic hybrid perovskite (C6H9N2)2MnI4. *Opt. Mater.* **2023**, *136*, 113360.
(43) Wang, Y.; Zhang, S.; Wang, Y.; Yan, J.; Yao, X.; Xu, M.; Lei, X.-w.; Lin, G.; Yue, C.-y. 0D triiodide hybrid halide perovskite for X-ray detection. *Chem. Commun.* **2023**, *59* (60), 9239−9242.
(44) Wang, D.-L.; Sun, D.-F.; Xu, L.-Y.; Liu, J.; Wang, J.-Y.; Shen, C.-Y. The synthesis, structure and photoluminescence of new (C8H18N)-2CdCl4 crystals. *J. Mol. Struct.* **2023**, *1282*, 135222.
(45) Teri, G.; Ni, H.-F.; Luo, Q.-F.; Wang, X.-P.; Wang, J.-Q.; Fu, D.-W.; Guo, Q. Tin-based organic−inorganic metal halides with a reversible phase transition and thermochromic response. *Mater. Chem. Front.* **2023**, *7* (11), 2235−2240.
(46) Sun, X.-Y.; Yue, M.; Jiang, Y.-X.; Zhao, C.-H.; Liao, Y.-Y.; Lei, X.-W.; Yue, C.-Y. Combining Dual-Light Emissions to Achieve Efficient Broadband Yellowish-Green Luminescence in One-Dimensional Hybrid Lead Halides. *Inorg. Chem.* **2021**, *60* (3), 1491−1498.
(47) Sun, C.; Guo, Y.-H.; Yuan, Y.; Chu, W.-X.; He, W.-L.; Che, H.-X.; Jing, Z.-H.; Yue, C.-Y.; Lei, X.-W. Broadband White-Light Emission in One-Dimensional Organic−Inorganic Hybrid Silver Halide. *Inorg. Chem.* **2020**, *59* (7), 4311−4319.
(48) Su, B.; Song, G.; Molokeev, M. S.; Lin, Z.; Xia, Z. Synthesis Crystal Structure and Green Luminescence in Zero-Dimensional Tin Halide (C8H14N2)2SnBr6. *Inorg. Chem.* **2020**, *59* (14), 9962−9968.
(49) Su, B.; Jin, J.; Peng, Y.; Molokeev, M. S.; Yang, X.; Xia, Z. Zero-Dimensional Organic Copper(I) Iodide Hybrid with High Anti-Water Stability for Blue-Light-Excitable Solid-State Lighting. *Adv. Opt. Mater.* **2022**, *10* (12), 2102619.
(50) Romagnoli, L.; D'Annibale, A.; Blundo, E.; Patra, A.; Polimeni, A.; Meggiolaro, D.; Andrusenko, I.; Marchetti, D.; Gemmi, M.; Latini, A. 4,4′-(Anthracene-9,10-diylbis(ethyne-2,1-diyl))bis(1-methyl-1-pyridinium) Lead Iodide C30H22N2Pb2I6: A Highly Luminescent, Chemically and Thermally Stable One-Dimensional Hybrid Iodoplumbate. *Chem. Mater.* **2023**, *35* (4), 1818−1826.
(51) Qi, Z.; Gao, H.; Zhu, X.; Lu, Z.; Zhang, X.-M. Blue Light-Excitable Broadband Yellow Emission in a Zero-Dimensional Hybrid Bismuth Halide with Type-II Band Alignment. *Inorg. Chem.* **2022**, *61* (48), 19483−19491.
(52) Qi, Z.; Gao, H.; Yang, X.; Chen, Y.; Zhang, F.-Q.; Qu, M.; Li, S.-L.; Zhang, X.-M. A One-Dimensional Broadband Emissive Hybrid Lead Iodide with Face-Sharing PbI6 Octahedral Chains. *Inorg. Chem.* **2021**, *60* (20), 15136−15140.
(53) Qi, Z.; Chen, Y.; Guo, Y.; Yang, X.; Zhang, F.-Q.; Zhou, G.; Zhang, X.-M. Broadband white-light emission in a one-dimensional organic−inorganic hybrid cadmium chloride with face-sharing CdCl6 octahedral chains. *J. Mater. Chem. C* **2021**, *9* (1), 88−94.
(54) Qi, S.; Cheng, P.; Han, X.; Ge, F.; Shi, R.; Xu, L.; Li, G.; Xu, J. Organic−Inorganic Hybrid Antimony(III) Halides for Second Harmonic Generation. *Cryst. Growth Des.* **2022**, *22* (11), 6545−6553.
(55) Peng, Y.-C.; Zhou, S.-H.; Jin, J.-C.; Zhuang, T.-H.; Gong, L.-K.; Lin, H.-W.; Wang, Z.-P.; Du, K.-Z.; Huang, X.-Y. [PPh3H]2[SbCl5]: A Zero-Dimensional Hybrid Metal Halide with a Supramolecular Framework and Stable Dual-Band Emission. *J. Phys. Chem. C* **2022**, *126* (40), 17381−17389.
(56) Peng, Y.; Yao, Y.; Li, L.; Wu, Z.; Wang, S.; Luo, J. White-light emission in a chiral one-dimensional organic−inorganic hybrid perovskite. *J. Mater. Chem. C* **2018**, *6* (22), 6033−6037.
(57) Peng, X.-L.; Han, R.-R.; Tang, Y.-Z.; Tan, Y.-H.; Fan, X.-W.; Wang, F.-X.; Zhang, H. 1D Chiral Lead Bromide Perovskite with Superior Second-Order Optical Nonlinearity, Photoluminescence, and High-Temperature Reversible Phase Transition. *Chem. − Asian J.* **2023**, *18* (4), No. e202201206.
(58) Peng, H.; Tian, Y.; Zhang, Z.; Wang, X.; Huang, T.; Dong, T.; Xiao, Y.; Wang, J.; Zou, B. Bulk Assembly of Zero-Dimensional Organic Copper Bromide Hybrid with Bright Self-Trapped Exciton Emission and High Antiwater Stability. *J. Phys. Chem. C* **2021**, *125* (36), 20014−20021.
(59) Peng, H.; Tian, Y.; Yu, Z.; Wang, X.; Ke, B.; Zhao, Y.; Dong, T.; Wang, J.; Zou, B. (C16H28N)2SbCl5: A new lead-free zero-dimensional metal-halide hybrid with bright orange emission. *Sci. China Mater.* **2022**, *65* (6), 1594−1600.
(60) Panda, D. P.; Swain, D.; Sarkar, S.; Sundaresan, A. Halogen Bond Induced Structural and Photophysical Properties Modification in Organic−Inorganic Hybrid Manganese Halides. *J. Phys. Chem. Lett.* **2023**, *14* (18), 4211−4218.
(61) Owczarek, M.; Lee, M.; Zapf, V.; Nie, W.; Jakubas, R. Accessing One-Dimensional Chains of Halogenoindates(III) in Organic−Inorganic Hybrids. *Inorg. Chem.* **2022**, *61* (14), 5469−5473.
(62) Molokeev, M. S.; Su, B.; Aleksandrovsky, A. S.; Golovnev, N. N.; Plyaskin, M. E.; Xia, Z. Machine Learning Analysis and Discovery of Zero-Dimensional ns2Metal Halides toward Enhanced Photoluminescence Quantum Yield. *Chem. Mater.* **2022**, *34* (2), 537−546.
(63) Maqbool, S.; Thekkayil, Z.; Mandal, P. 1D Diisopropylammonium Lead Iodide Perovskite Shows Exceptional Optical Stability and Third-Order Nonlinearity. *Adv. Opt. Mater.* **2023**, *11* (15), 2202942.
(64) Mao, L.; Guo, P.; Kepenekian, M.; Hadar, I.; Katan, C.; Even, J.; Schaller, R. D.; Stoumpos, C. C.; Kanatzidis, M. G. Structural Diversity in White-Light-Emitting Hybrid Lead Bromide Perovskites. *J. Am. Chem. Soc.* **2018**, *140* (40), 13078−13088.
(65) Liu, Y.-H.; Wang, W.-Q.; Zhang, B.-L.; Wang, Y.-J.; Ren, M.-P.; Jing, Z.; Yue, C.-Y. Zero-dimensional organic−inorganic hybrid zinc halide with broadband yellow light emission. *CrystEngComm* **2023**, *25* (3), 444−449.
(66) Liu, Y.-H.; Wang, N.-N.; Ren, M.-P.; Yan, X.; Wu, Y.-F.; Yue, C.-Y.; Lei, X.-W. Zero-Dimensional Hybrid Cuprous Halide of [BAPMA]-Cu2Br5 as a Highly Efficient Light Emitter and an X-Ray Scintillator. *ACS Appl. Mater. Interfaces* **2023**, *15* (16), 20219−20227.
(67) Liu, X.; Li, Y.; Liang, T.; Fan, J. Role of Polyhedron Unit in Distinct Photophysics of Zero-Dimensional Organic−Inorganic Hybrid Tin Halide Compounds. *J. Phys. Chem. Lett.* **2021**, *12* (24), 5765−5773.
(68) Liu, W.-T.; Zhang, Z.-X.; Ding, K.; Fu, D.-W.; Lu, H.-F. Halogen tuning toward dielectric switch and band gap engineering in one-dimensional hybrid materials. *J. Mol. Struct.* **2022**, *1270*, 133954.
(69) Liu, S.; Fang, X.; Lu, B.; Yan, D. Wide range zero-thermal-quenching ultralong phosphorescence from zero-dimensional metal halide hybrids. *Nat. Commun.* **2020**, *11* (1), 4649.
(70) Liu, K.; Hao, S.; Cao, J.; Lin, J.; Fan, L.; Zhang, X.; Guo, Z.; Wolverton, C.; Zhao, J.; Liu, Q. Antimony doping to enhance luminescence of tin(iv)-based hybrid metal halides. *Inorg. Chem. Front.* **2022**, *9* (15), 3865−3873.
(71) Liu, F.; Mondal, D.; Zhang, K.; Zhang, Y.; Huang, K.; Wang, D.; Yang, W.; Mahadevan, P.; Xie, R. Zero-dimensional plate-shaped copper halide crystals with green-yellow emissions. *Mater. Adv.* **2021**, *2* (11), 3744−3751.
(72) Lin, J.; Liu, K.; Ruan, H.; Sun, N.; Chen, X.; Zhao, J.; Guo, Z.; Liu, Q.; Yuan, W. Zero-Dimensional Lead-Free Halide with Indirect Optical Gap and Enhanced Photoluminescence by Sb Doping. *J. Phys. Chem. Lett.* **2022**, *13* (1), 198−207.
(73) Lin, H.; Zhou, C.; Neu, J.; Zhou, Y.; Han, D.; Chen, S.; Worku, M.; Chaaban, M.; Lee, S.; Berkwits, E.; et al. Bulk Assembly of Corrugated 1D Metal Halides with Broadband Yellow Emission. *Adv. Opt. Mater.* **2019**, *7* (6), 1801474.
(74) Lin, H.; Zhou, C.; Chaaban, M.; Xu, L.-J.; Zhou, Y.; Neu, J.; Worku, M.; Berkwits, E.; He, Q.; Lee, S.; et al. Bulk Assembly of Zero-Dimensional Organic Lead Bromide Hybrid with Efficient Blue Emission. *ACS Mater. Lett.* **2019**, *1* (6), 594−598.
(75) Lin, F.; Yu, G.; Weng, S.; Zhou, C.; Han, Y.; Liu, W.; Zhou, K.; Wang, Y.; Lin, H. Blue photoluminescence enhancement achieved by zero-dimensional organic indium halides via a metal ion doping strategy. *Mater. Chem. Front.* **2022**, *7* (1), 137−144.
(76) Lian, L.; Zhang, T.; Ding, H.; Zhang, P.; Zhang, X.; Zhao, Y.-B.; Gao, J.; Zhang, D.; Zhao, Y. S.; Zhang, J. Highly Luminescent Zero-Dimensional Organic Copper Halide with Low-Loss Optical Wave-

https://doi.org/10.1021/acs.chemmater.5c02573
Chem. Mater. XXXX, XXX, XXX−XXX

guides and Highly Polarized Emission. *ACS Mater. Lett.* **2022**, *4* (8), 1446−1452.
(77) Li, P.-F.; Liao, W.-Q.; Tang, Y.-Y.; Ye, H.-Y.; Zhang, Y.; Xiong, R.-G. Unprecedented Ferroelectric−Antiferroelectric−Paraelectric Phase Transitions Discovered in an Organic−Inorganic Hybrid Perovskite. *J. Am. Chem. Soc.* **2017**, *139* (25), 8752−8757.
(78) Li, M.; Lin, J.; Liu, K.; Fan, L.; Wang, N.; Guo, Z.; Yuan, W.; Zhao, J.; Liu, Q. Light-Emitting 0D Hybrid Metal Halide (C3H12N2)-2Sb2Cl10 with Antimony Dimers. *Inorg. Chem.* **2021**, *60* (15), 11429−11434.
(79) Li, L.-S.; Tan, Y.-H.; Wei, W.-J.; Gao, H.-Q.; Tang, Y.-Z.; Han, X.-B. Chiral Switchable Low-Dimensional Perovskite Ferroelectrics. *ACS Appl. Mater. Interfaces* **2021**, *13* (1), 2044−2051.
(80) Li, K.-J.; Zhao, Y.-Y.; Sun, M.-E.; Chen, G.-S.; Zhang, C.; Liu, H.-L.; Li, H.-Y.; Zang, S.-Q.; Mak, T. C. W. Zero-Dimensional Zinc Halide Organic Hybrids with Excellent Optical Waveguide Properties. *Cryst. Growth Des.* **2022**, *22* (5), 3295−3302.
(81) Li, D. Y.; Liu, Y. H.; Wang, Q.; Lei, X. W.; Yue, C. Y.; Jing, Z. H. Zero-dimensional hybrid zinc halides with blue light emissions. *Mater. Today Chem.* **2023**, *31*, 101604.
(82) Li, D.-F.; Zhao, P.-J.; Deng, X.-H.; Wu, Y.-Z.; He, X.-L.; Liu, D.-S.; Li, Y.-X.; Sui, Y. A new organic−inorganic hybrid perovskite ferroelectric [ClCH2CH2N(CH3)3][PbBr3] and Its PVDF matrix-assisted highly-oriented flexible ferroelectric films. *New J. Chem.* **2022**, *46* (40), 19391−19400.
(83) Li, B.; Xu, Y.; Zhang, X.; Han, K.; Jin, J.; Xia, Z. Zero-Dimensional Luminescent Metal Halide Hybrids Enabling Bulk Transparent Medium as Large-Area X-Ray Scintillators. *Adv. Opt. Mater.* **2022**, *10* (10), 2102793.
(84) Li, B.; Jin, J.; Yin, M.; Zhang, X.; Molokeev, M. S.; Xia, Z.; Xu, Y. Sequential and Reversible Phase Transformations in Zero-Dimensional Organic-Inorganic Hybrid Sb-based Halides towards Multiple Emissions. *Angew. Chem., Int. Ed.* **2022**, *134* (49), No. e202212741.
(85) Lee, T.; Straus, D. B.; Xu, X.; Xie, W.; Cava, R. J. Tunable Magnetic Transition Temperatures in Organic−Inorganic Hybrid Cobalt Chloride Hexagonal Perovskites. *Chem. Mater.* **2023**, *35* (4), 1745−1751.
(86) Klee, P. S.; Hirano, Y.; Cordes, D. B.; Slawin, A. M. Z.; Payne, J. L. Synthesis, Structure, and Tunability of Zero-Dimensional Organic−Inorganic Metal Halides Utilizing the m-Xylylenediammonium Cation: MXD2PbI6, MXDBiI5, and MXD3Bi2Br12·2H2O. *Cryst. Growth Des.* **2022**, *22* (6), 3815−3823.
(87) Jiang, X.; Chen, Z.; Tao, X. $(1\text{-}C5H14N2Br)_2MnBr_4$: A Lead-Free Zero-Dimensional Organic-Metal Halide With Intense Green Photoluminescence. *Front. Chem.* **2020**, *8*, 352.
(88) He, S.; Hao, S.; Fan, L.; Liu, K.; Cai, C.; Wolverton, C.; Zhao, J.; Liu, Q. Efficient Solar Spectrum-Like White-Light Emission in Zinc-Based Zero-Dimensional Hybrid Metal Halides. *Adv. Opt. Mater.* **2023**, *11* (15), 2300218.
(89) Gao, H.; Lu, Z.; Zhao, X.; Zhang, K.; Zhu, X.; Cheng, R.; Li, S.-L.; Qi, Z.; Zhang, X.-M. Singlet exciton and singlet/triplet self-trapped excitons for ultra-broadband white-light emission in a zero-dimensional cadmium bromide hybrid. *J. Mater. Chem. C* **2023**, *11* (26), 9023−9029.
(90) Fang, H.; Chen, F.-H.; Zhang, S.-Q.; Lin, M.-J. Three Semiconductive 1D Naphthalene Diimide/Iodoplumbate Perovskites with High Moisture Tolerance and Long-Lived Charge Separation States. *Inorg. Chem.* **2023**, *62* (24), 9661−9670.
(91) Fan, L.; Hao, S.; He, S.; Zhang, X.; Li, M.; Wolverton, C.; Zhao, J.; Liu, Q. Luminescent hybrid halides with various centering metal cations (Zn, Cd and Pb) and diverse structures. *Dalton Trans.* **2023**, *52* (16), 5119−5126.
(92) Fabian, D. M.; Ganose, A. M.; Ziller, J. W.; Scanlon, D. O.; Beard, M. C.; Ardo, S. Influence of One Specific Carbon−Carbon Bond on the Quality, Stability, and Photovoltaic Performance of Hybrid Organic−Inorganic Bismuth Iodide Materials. *ACS Appl. Energy Mater.* **2019**, *2* (3), 1579−1587.
(93) Du, Y.; Ma, L.; Yan, Z.; Xiao, J.; Wang, K.; Lin, T.; Han, X.; Xia, D. One-Dimensional Hybrid Copper(I) Iodide Single Crystal with Renewable Scintillation Properties. *Inorg. Chem.* **2023**, *62* (29), 11350−11359.
(94) Creason, T. D.; Fattal, H.; Gilley, I. W.; Evans, B. N.; Jiang, J.; Pachter, R.; Glatzhofer, D. T.; Saparov, B. Stabilized photoemission from organic molecules in zero-dimensional hybrid Zn and Cd halides. *Inorg. Chem. Front.* **2022**, *9* (23), 6202−6210.
(95) Cheng, X.; Yue, S.; Chen, R.; Yin, J.; Cui, B.-B. White Light-Emitting Diodes Based on One-Dimensional Organic−Inorganic Hybrid Metal Chloride with Dual Emission. *Inorg. Chem.* **2022**, *61* (39), 15475−15483.
(96) Chen, R.; Sun, C.; Cheng, X.; Lin, Y.; Zhou, J.; Yin, J.; Cui, B.-B.; Mao, L. One-Dimensional Organic−Inorganic Lead Bromide Hybrids with Excitation-Dependent White-Light Emission Templated by Pyridinium Derivatives. *Inorg. Chem.* **2023**, *62* (24), 9722−9731.
(97) Chen, Q.; Dai, F.; Zhang, K.; Zhou, H.; Zhang, M.; Quan, D.; Wang, L.; Xing, J. Synthesis crystal structure and white luminescence of zero-dimensional organic−inorganic zinc halides. *J. Mater. Chem. C* **2022**, *10* (48), 18279−18284.
(98) Chai, C.-Y.; Han, X.-B.; Liu, C.-D.; Fan, C.-C.; Liang, B.-D.; Zhang, W. Circularly Polarized Luminescence in Zero-Dimensional Antimony Halides: Structural Distortion Controlled Luminescence Thermometer. *J. Phys. Chem. Lett.* **2023**, *14* (17), 4063−4070.
(99) Biswas, A.; Bakthavatsalam, R.; Bahadur, V.; Biswas, C.; Mali, B. P.; Raavi, S. S. K.; Gonnade, R. G.; Kundu, J. Lead-free zero dimensional tellurium(iv) chloride-organic hybrid with strong room temperature emission as a luminescent material. *J. Mater. Chem. C* **2021**, *9* (12), 4351−4358.
(100) Bi, W.; Mercier, N. Reversible dynamic isomerism change in the solid state, from Bi4I16clusters to BiI4 1D chains in l-cystine based hybrids: templating effect of cations in iodobismuthate network formation. *Chem. Commun.* **2008**, *44*, 5743−5745.
(101) Lin, H.; Zhou, C.; Tian, Y.; Besara, T.; Neu, J.; Siegrist, T.; Zhou, Y.; Bullock, J.; Schanze, K. S.; Ming, W.; et al. Bulk assembly of organic metal halide nanotubes. *Chem. Sci.* **2017**, *8* (12), 8400−8404.
(102) Lee, S.; Karkee, R.; Ben-Akacha, A.; Luong, D.; Vellore Winfred, J. S. R.; Lin, X.; Strubbe, D. A.; Ma, B. One-dimensional organic metal halide nanoribbons with dual emission. *Chem. Commun.* **2023**, *59* (25), 3711−3714.
(103) Zhou, C.; Lin, H.; Neu, J.; Zhou, Y.; Chaaban, M.; Lee, S.; Worku, M.; Chen, B.; Clark, R.; Cheng, W.; et al. Green Emitting Single-Crystalline Bulk Assembly of Metal Halide Clusters with Near-Unity Photoluminescence Quantum Efficiency. *ACS Energy Lett.* **2019**, *4* (7), 1579−1583.
(104) Zhou, C.; Lin, H.; Worku, M.; Neu, J.; Zhou, Y.; Tian, Y.; Lee, S.; Djurovich, P.; Siegrist, T.; Ma, B. Blue Emitting Single Crystalline Assembly of Metal Halide Clusters. *J. Am. Chem. Soc.* **2018**, *140* (41), 13181−13184.
(105) Chen, Z.; Xue, J.; Wang, Z.; Lu, H. Magnetic hybrid transition metal halides. *Mater. Chem. Front.* **2023**, *8* (1), 210−227.
(106) Chen, Y.; Lun, Z.; Zhao, X.; Koirala, K. P.; Li, L.; Sun, Y.; O'Keefe, C. A.; Yang, X.; Cai, Z.; Wang, C.; et al. Unlocking Li superionic conductivity in face-centred cubic oxides via face-sharing configurations. *Nat. Mater.* **2024**, *23* (4), 535−542.
(107) Wang, L.; Wang, Y.; Martin, J.; Scivally, E.; He, Z.; Kim, D.-h.; Yeon, D.-h.; Zeng, Y.; Chen, D.; Ouyang, B. Origin of enhanced disorder in high entropy rocksalt type Li-ion battery cathodes. *EES Batteries* **2025**, *1*, 1731.
(108) Lun, Z.; Ouyang, B.; Kwon, D.-H.; Ha, Y.; Foley, E. E.; Huang, T.-Y.; Cai, Z.; Kim, H.; Balasubramanian, M.; Sun, Y.; et al. Cation-disordered rocksalt-type high-entropy cathodes for Li-ion batteries. *Nat. Mater.* **2021**, *20* (2), 214−221.
(109) He, Y.; Islam, M. S.; Viera, J.; Gao, H.; Sun, J.; Ma, B.; Ouyang, B. Identifying Practical DFT Functionals for Predicting 0D and 1D Organic Metal-Halide Hybrids. *J. Phys. Chem. C* **2024**, *128* (42), 17850−17858.
(110) Jain, A.; Shin, Y.; Persson, K. A. Computational predictions of energy materials using density functional theory. *Nat. Rev. Mater.* **2016**, *1* (1), 15004.

https://doi.org/10.1021/acs.chemmater.5c02573
Chem. Mater. XXXX, XXX, XXX−XXX

(111) Amira, S.; Spångberg, D.; Hermansson, K. OD vibrations and hydration structure in an Al3+(aq) solution from a Car-Parrinello molecular-dynamics simulation. *J. Chem. Phys.* **2006**, *124* (10), 104501.
(112) Pasquarello, A.; Petri, I.; Salmon, P. S.; Parisel, O.; Car, R.; Tóth, E.ˊ.; Powell, D. H.; Fischer, H. E.; Helm, L.; Merbach, A. E. First Solvation Shell of the Cu(II) Aqua Ion: Evidence for Fivefold Coordination. *Science* **2001**, *291* (5505), 856−859.
(113) Benedek, R.; Thackeray, M. M. Reaction Energy for LiMn2O4 Spinel Dissolution in Acid. *Electrochem. Solid-State Lett.* **2006**, *9* (6), A265.
(114) Benedek, R.; van de Walle, A. Free Energies for Acid Attack Reactions of Lithium Cobaltate. *J. Electrochem. Soc.* **2008**, *155* (10), A711.
(115) Gillan, M. J.; Alfè, D.; Michaelides, A. Perspective: How good is DFT for water? *J. Chem. Phys.* **2016**, *144* (13), 130901.
(116) Sun, W.; Kitchaev, D. A.; Kramer, D.; Ceder, G. Non-equilibrium crystallization pathways of manganese oxides in aqueous solution. *Nat. Commun.* **2019**, *10* (1), 573.
(117) Persson, K. A.; Waldwick, B.; Lazic, P.; Ceder, G. Prediction of solid-aqueous equilibria: Scheme to combine first-principles calculations of solids with experimental aqueous states. *Phys. Rev. B* **2012**, *85* (23), 235438.
(118) Ouyang, B.; Wang, J.; He, T.; Bartel, C. J.; Huo, H.; Wang, Y.; Lacivita, V.; Kim, H.; Ceder, G. Synthetic accessibility and stability rules of NASICONs. *Nat. Commun.* **2021**, *12* (1), 5752.
(119) Johnson, J. W.; Oelkers, E. H.; Helgeson, H. C. SUPCRT92: A software package for calculating the standard molal thermodynamic properties of minerals, gases, aqueous species, and reactions from 1 to 5000 bar and 0 to 1000°C. *Comput. Geosci.* **1992**, *18* (7), 899−947.
(120) Kresse, G.; Furthmüller, J. Efficiency of ab-initio total energy calculations for metals and semiconductors using a plane-wave basis set. *Comput. Mater. Sci.* **1996**, *6* (1), 15−50.
(121) Kresse, G.; Hafner, J. Ab initio molecular-dynamics simulation of the liquid-metal−amorphous-semiconductor transition in germanium. *Phys. Rev. B* **1994**, *49* (20), 14251.
(122) Kresse, G.; Hafner, J. Ab initio molecular dynamics for liquid metals. *Phys. Rev. B* **1993**, *47* (1), 558.
(123) Perdew, J. P.; Burke, K.; Ernzerhof, M. Generalized gradient approximation made simple. *Phys. Rev. Lett.* **1996**, *77* (18), 3865.
(124) Blöchl, P. E. Projector augmented-wave method. *Phys. Rev. B* **1994**, *50* (24), 17953.
(125) Kresse, G.; Joubert, D. From ultrasoft pseudopotentials to the projector augmented-wave method. *Phys. Rev. B* **1999**, *59* (3), 1758.
(126) Monkhorst, H. J.; Pack, J. D. Special points for Brillouin-zone integrations. *Phys. Rev. B* **1976**, *13* (12), 5188−5192.
(127) Methfessel, M.; Paxton, A. T. High-precision sampling for Brillouin-zone integration in metals. *Phys. Rev. B* **1989**, *40* (6), 3616−3621.
(128) Wang, L.; Maxisch, T.; Ceder, G. Oxidation energies of transition metal oxides within the $\mathrm{GGA}+\mathrm{U}$ framework. *Phys. Rev. B* **2006**, *73* (19), 195107.
(129) Dudarev, S. L.; Botton, G. A.; Savrasov, S. Y.; Humphreys, C. J.; Sutton, A. P. Electron-energy-loss spectra and the structural stability of nickel oxide: An LSDA+U study. *Phys. Rev. B* **1998**, *57* (3), 1505−1509.
(130) Ong, S. P.; Richards, W. D.; Jain, A.; Hautier, G.; Kocher, M.; Cholia, S.; Gunter, D.; Chevrier, V. L.; Persson, K. A.; Ceder, G. Python Materials Genomics (pymatgen): A robust, open-source python library for materials analysis. *Comput. Mater. Sci.* **2013**, *68*, 314−319.
(131) Dolomanov, O. V.; Bourhis, L. J.; Gildea, R. J.; Howard, J. A. K.; Puschmann, H. OLEX2: a complete structure solution, refinement and analysis program. *J. Appl. Crystallogr.* **2009**, *42* (2), 339−341.
(132) Sheldrick, G. Crystal structure refinement with SHELXL. *Acta Crystallogr., Sect. C:Struct. Chem.* **2015**, *71* (1), 3−8.

https://doi.org/10.1021/acs.chemmater.5c02573
Chem. Mater. XXXX, XXX, XXX−XXX